Wide distribution and glacial origin of polar gypsum on Mars

M. Massé [a,b,*], O. Bourgeois [a], S. Le Mouélic [a], C. Verpoorter [c], A. Spiga [d], L. Le Deit [e]

[a] *Laboratoire de Planétologie et Géodynamique, UMR 6112, CNRS, Université de Nantes, 2 chemin de la Houssinière, BP 92205, 44322 Nantes Cedex 3, France*
[b] *Lunar and Planetary Laboratory, University of Arizona, 1629 E. University Blvd., Tucson, AZ 85721-0092,USA*
[c] *Limnology, Department of Ecology and Evolution, University of Uppsala, Norbyägen 18D, SE-75236 Uppsala, Sweden*
[d] *Laboratoire de Météorologie Dynamique, Université Pierre et Marie Curie, Paris, France*
[e] *Institute of Planetary Research, German Aerospace Center (DLR), Rutherfordstr.2, 12489 Berlin, Germany*

ABSTRACT

The North Polar Cap of Mars is associated with different kinds of superficial sediments, including the Circumpolar Dune Field, interior dune fields and sedimentary veneers scattered over the ice cap. In order to resolve the mineralogical composition and the regional distribution of these sediments, we processed OMEGA and CRISM hyperspectral data with an original method based on spectral derivation. We find that gypsum is present in all areas where undefined hydrated minerals had been previously detected, including superficial sedimentary veneers covering the North Polar Cap, interior dune fields and the whole Circumpolar Dune Field. Morphological and structural analyses reveal that these gypsum crystals derive directly from the interior of the ice cap. The source of superficial sedimentary veneers is the dust that was previously contained in the upper part of the ice cap, the ice-rich North Polar Layered Deposits (NPLD). This gypsum-bearing dust was released, on south-facing slopes of spiral troughs and arcuate scarps, by ice ablation controlled by katabatic winds. By the analysis of all associations of erosional scarps and dune fields over the North Polar Cap, we also demonstrate that the polar dunes are composed of sand-sized particles that were previously contained in the sediment-rich Basal Unit (BU), corresponding to the lower part of the ice cap. These particles contain gypsum and were released from the BU, by regressive ablation of ice at marginal scarps that border the North Polar Cap and by vertical ablation of ice on Olympia Planum. From a reconstruction of wind streamlines over and around the ice cap, we infer that katabatic winds descending from the polar high and rotating around the North Polar Cap control the release of these gypsum-bearing particles by ice ablation and the redistribution of these particles in the Circumpolar Dune Field.

© 2011 Elsevier B.V. All rights reserved.

1. Introduction

One of the most intriguing recent discoveries in the polar regions of Mars is the presence of extensive deposits of gypsum, a hydrated calcium sulfate ($CaSO_4 \cdot 2H_2O$), close to the North Polar Cap. These were detected in Olympia Planum, a portion of the Circumpolar Dune Field (Figs.1a and 2; Fishbaugh et al., 2007; Tanaka and Hayward, 2008), first by the OMEGA imaging spectrometer (Langevin et al., 2005a) and later by the CRISM imaging spectrometer (Roach et al., 2007). From complementary CRISM and OMEGA hyperspectral data, it was shown that gypsum is also present in other parts of the Circumpolar Dune Field and on the North Polar Cap itself (Massé et al., 2010).

Various hypotheses have been suggested for the origin of these polar gypsum deposits. Because of its softness, gypsum is easily susceptible to physical weathering; therefore the gypsum detected around the North Polar Cap has probably formed in-situ or within a short distance from its current location (Fishbaugh et al., 2007). On this basis, Langevin et al. (2005a) suggested two different hypotheses for its formation: interaction of Ca-rich minerals with snow containing H_2SO_4 derived from volcanic activity or formation as an evaporite deposit after major meltwater outflows from the ice cap during warm climatic incursions. Fishbaugh et al. (2007) suggested that water from nearby channels percolated through dunes that cover the eastern end of Olympia Planum and attributed the formation of gypsum there to a combination of (1) in-situ aqueous weathering of sulfide- and high-calcium-pyroxene-bearing dune materials and (2) formation of evaporitic gypsum crystals in the pore spaces of these materials. Szynkiewicz et al. (2010) suggested that gypsum crystals were formed by evaporation of saline waters and were later transported by winds toward Olympia Planum. Alternatively, it has been suggested that gypsum crystals could derive directly from the sediment-rich Basal Unit of the North Polar Cap (Fig. 1b) (Calvin et al., 2009; Roach et al., 2007).

* Corresponding author at: Laboratoire de Planétologie et Géodynamique, UMR 6112, CNRS, Université de Nantes, 2 chemin de la Houssinière, BP 92205, 44322 Nantes Cedex 3, France.

E-mail addresses: marion.masse@univ-nantes.fr, marionmasse@pirl.lpl.arizona.edu (M. Massé), olivier.bourgeois@univ-nantes.fr (O. Bourgeois), stephane.lemouelic@univ-nantes.fr (S. Le Mouélic), Charles.Verpoorter@ebc.uu.se (C. Verpoorter), aymeric.spiga@upmc.fr (A. Spiga), Laetitia.LeDeit@dlr.de (L. Le Deit).
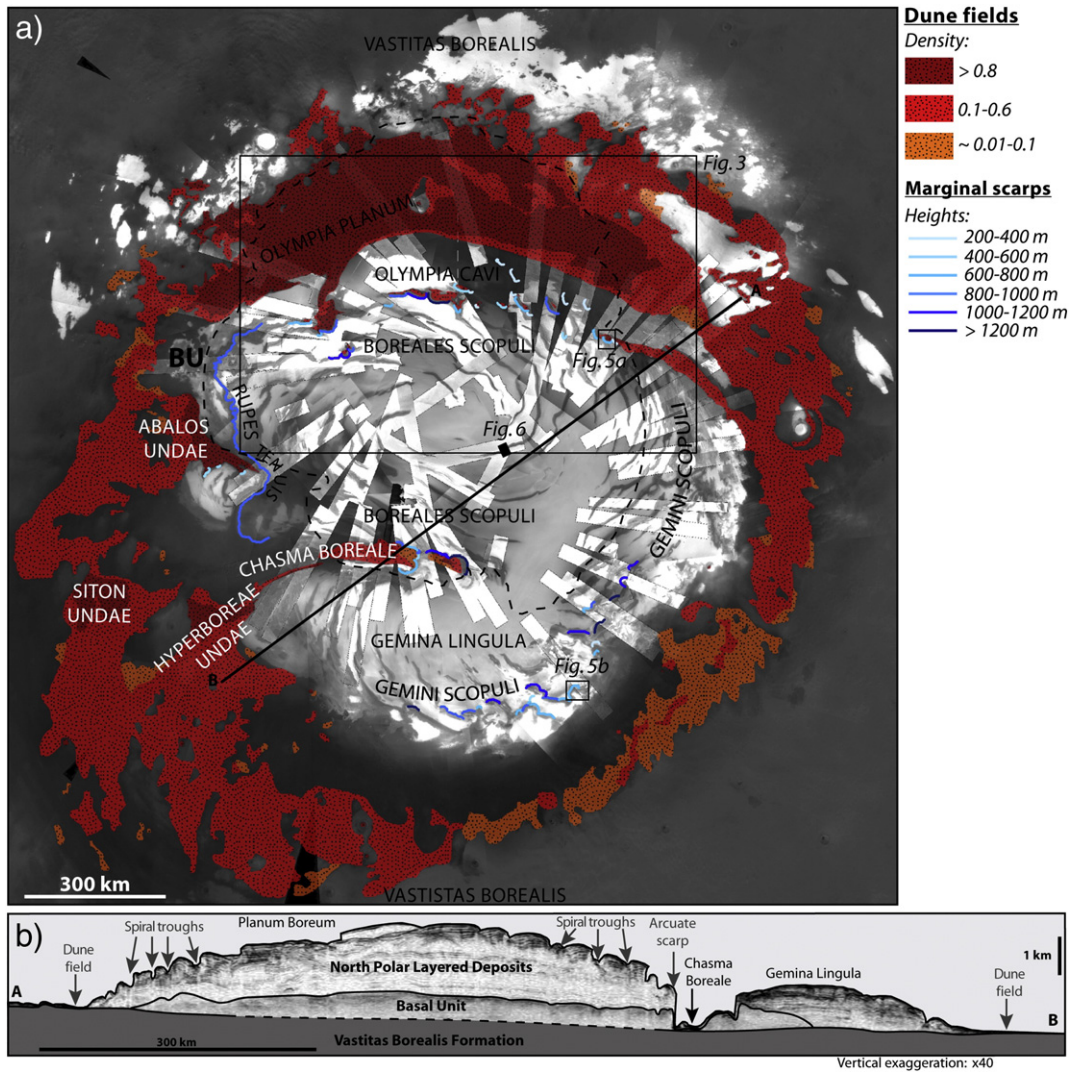
Fig. 1. a) Map of the North Polar Cap and Circumpolar Dune Field on a global MOC and CTX mosaic. Red, orange and yellow areas correspond to the Circumpolar Dune Field, ordered from the highest to the lowest dune density (modified from Tanaka and Hayward, 2008). Blue lines delineate North Polar marginal scarps and the blue scale represents the height of these scarps. The black stippled line represents the extension of the Basal Unit (BU) inferred from radar soundings by Selvans et al. (2010). b) Interpretative cross-section of the North Polar Cap (location indicated by a black line in a) based on SHARAD radargrams (Putzig et al., 2009). The dotted line indicates the top of the Vastitas Borealis Formation (VBF), as interpreted from scarce radar returns. Black boxes indicate locations of Figs. 3, 5 and 6.

In a restricted area located at the margin of the North Polar Cap, Massé et al. (2010) demonstrated that gypsum crystals that are now present in circumpolar dunes were originally trapped within the ice layers of the North Polar Cap and have been released by sublimation of the ice. On the basis of comparisons with sulfates present in terrestrial glaciers (Iizuka et al., 2006, 2008; Ohno et al., 2006), Massé et al. (2010) suggested that gypsum crystals trapped in the North Polar Cap had formed initially by weathering of dust particles, either in the atmosphere prior to their deposition during the formation of the ice cap, and/or in the ice cap after their deposition.

The present study aims at going a step further by mapping the distribution of north polar gypsum on a regional scale, so as to better constrain its origin and the processes by which gypsum crystals are released from the North Polar Cap and transferred toward the Circumpolar Dune Field. For that purpose we performed a morphological and compositional analysis of different kinds of superficial sediments associated to the North Polar Cap: (1) the Circumpolar Dune Field as a whole, (2) smaller interior dune fields associated with scarps cutting through the polar cap margin and (3) superficial sedimentary veneers covering the surface of the polar cap. We also reconstructed wind streamlines over the North Polar Cap and the Circumpolar Dune Field. On the basis of this reconstruction, we show how katabatic winds descending from the polar high and rotating around the ice cap control the release of gypsum from the ice and its redistribution in the Circumpolar Dune Field.

2. Geological setting

The North Polar Cap rests in the lowest part of the Vastitas Borealis topographic basin (Fig. 1a and b). It is 1300 km in diameter and reaches a maximum thickness of 3 km at its center (Zuber et al., 1998). The formation of the whole ice cap took place during the Amazonian (Carr and Head, 2009). It is a stack of water ice layers containing various amounts of intermixed sediment (dust and/or sand) (Fishbaugh et al., 2008; Howard et al., 1982; Kieffer et al., 1976; Tsoar et al., 1979).

Two distinct units have been recognized in this stack (Fig. 1b). The first one corresponds to the Basal Unit (BU), which rests directly on the Vastitas Borealis Formation (VBF). High-resolution images reveal that the BU consists of a low albedo, 1 km-thick formation displaying platy interbedded sequences of ice-rich and sediment-rich layers (Byrne and Murray, 2002; Edgett et al., 2003; Fishbaugh and Head,
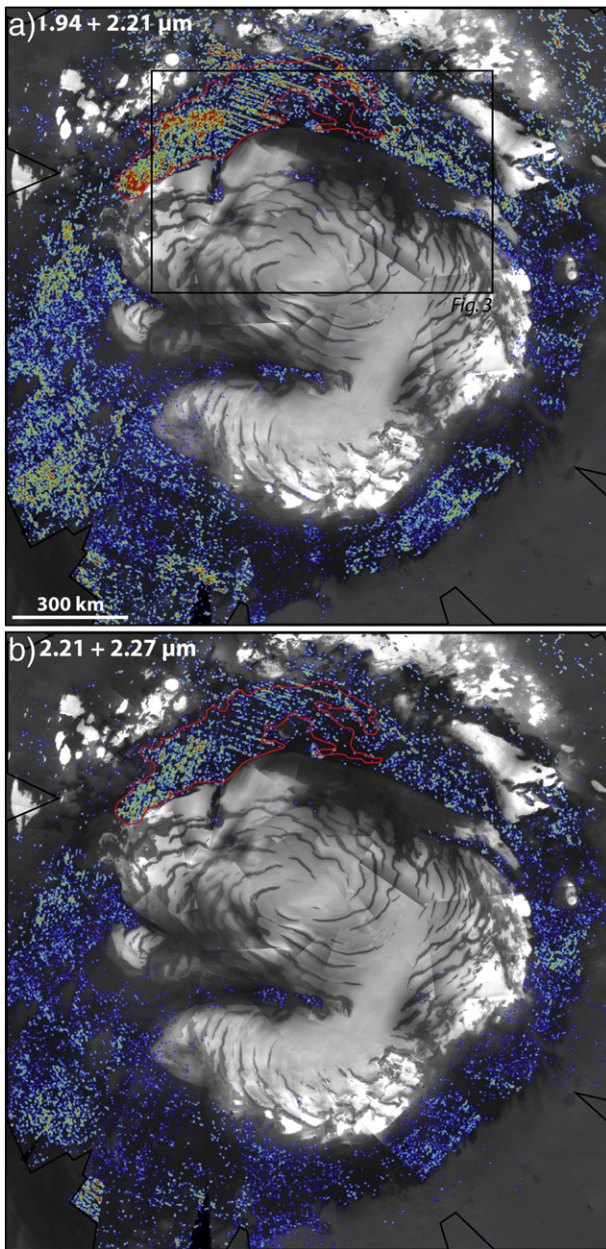
Fig. 2. Distribution of gypsum computed by the spectral derivative method (Massé et al., 2010) on a regional mosaic of OMEGA cubes. The extent of the regional mosaic is outlined by a black contour. Colored pixels correspond to pixels where the spectrum displays local minima simultaneously at 1.94 and 2.21 μm (on a) and at 2.21 and 2.27 μm (on b). Colors represent the number of pixels (1 to 9 pixels from blue to red) where this minimum is detected in a moving kernel of 3×3 pixels. The area where gypsum was previously detected by Langevin et al. (2005a) is outlined in red.

layers and ~30% for a few strong radar reflective layers (Grima et al., 2009; Phillips et al., 2008; Picardi et al., 2005; Selvans et al., 2010). On the basis of morphological and sedimentological interpretations of high-resolution images, Tanaka et al. (2008) further subdivided the BU and the NPLD into a full suite of stratigraphic units.

The surface morphology of the North Polar Cap is dominated by interior spiral troughs and marginal scarps (Howard, 2000) (Fig. 1a and b). These spiral troughs and scarps provide natural cross-sections where the internal structure of the North Polar Cap can be observed. Spiral troughs only cut through the NPLD and do not reach the BU (Putzig et al., 2009). The most convincing hypothesis
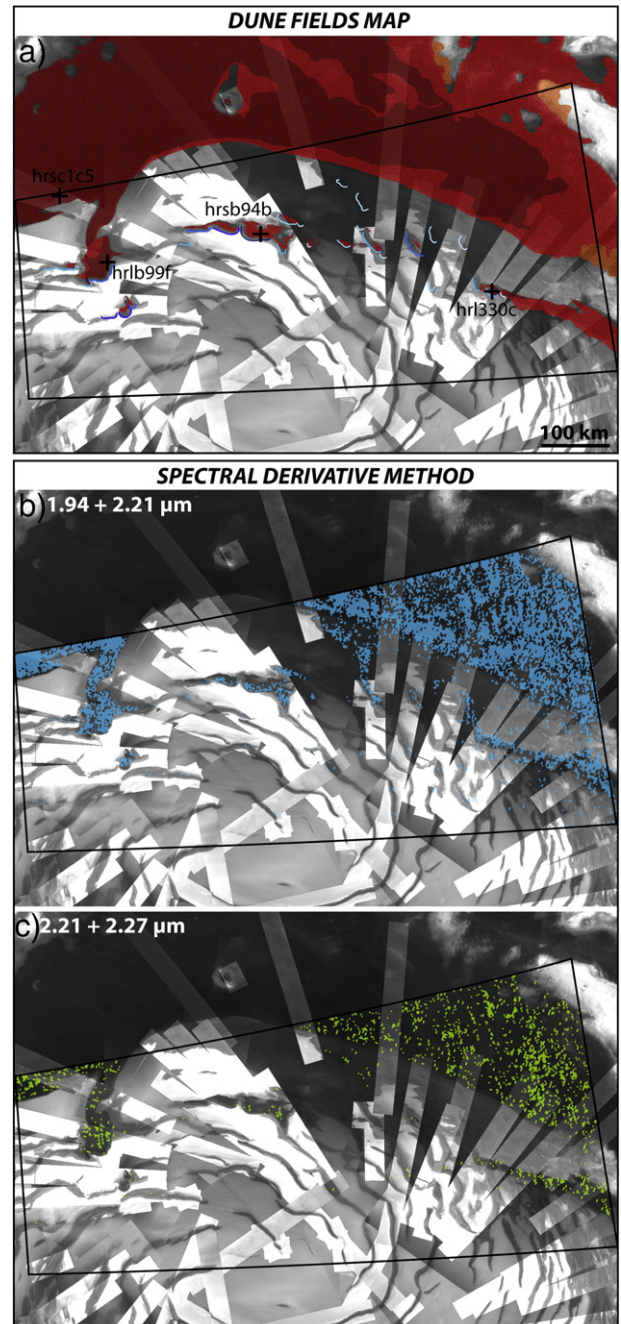

Fig. 3. Detection of gypsum in interior dune fields. a) Map of interior dune fields and marginal scarps (location indicated by a black box in Fig. 1a, same legend and color scale than Fig. 1a). b) and c) Distribution of gypsum computed by the spectral derivative method on OMEGA cube # 1030_2. Pixels where the spectrum meets local minima simultaneously at 1.94 and 2.21 μm (b) and at 2.21 and 2.27 μm (c) are colored respectively in blue and green.

2005). SHARAD and MARSIS radar soundings have confirmed the existence of this sediment-rich BU, and have revealed that it is largely confined to the major lobe of the North Polar Cap (Fig. 1a) (Phillips et al., 2008; Picardi et al., 2005; Putzig et al., 2009; Selvans et al., 2010). The second unit corresponds to the upper (and younger) part of the ice cap, which is composed of the North Polar Layered Deposits (NPLD). On high-resolution images, the NPLD appear brighter and more finely layered than the BU. The majority of the NPLD is made of water ice and their layering results from varying fractions of included sediment and/or varying ice grain sizes (Calvin et al., 2009; Kieffer et al., 1976). Radar soundings have confirmed that the amount of sediment in the NPLD is small, with only ~2% for most

for their formation is by a combination of ice ablation (due to katabatic winds and sublimation) on their equator-facing slopes and ice deposition on their pole-facing slopes (Howard, 1978; Howard, 2000; Ivanov and Muhleman, 2000; Ng and Zuber, 2006; Smith and Holt, 2010). Ablation by katabatic winds and sublimation are most probably responsible for the formation of the marginal scarps also (Massé et al., 2010; Warner and Farmer, 2008).

In addition to sediments intermixed in the ice of the BU and of the NPLD, polar sediments also exist in the form of:

(1) dunes constituting the Circumpolar Dune Field;
(2) smaller interior dune fields covering the ice cap and associated with marginal scarps;
(3) superficial sedimentary veneers covering the surface of the NPLD, particularly in spiral troughs.

Constraints on the composition of these various kinds of polar superficial sediments have been provided by the OMEGA and CRISM imaging spectrometers. Gypsum has been detected in the dunes of Olympia Planum (Langevin et al., 2005a; Roach et al., 2007) and in superficial sediments associated to a marginal scarp located at the longitude of 118°E between Olympia Cavi and Gemini Scopuli (Massé et al., 2010). Signatures of hydrated and mafic minerals have been detected on the rest of the polar superficial sediments (Calvin et al., 2009; Horgan et al., 2009; Poulet et al., 2008). However, it is unclear whether the signatures of hydrated minerals correspond to gypsum, to another kind of hydrated sulfate or more generally to any other hydrated mineral. In our regional study, we investigate over the whole Circumpolar Dune Field and over the whole North Polar Cap whether these signatures of hydrated minerals correspond to gypsum or not.

3. Data and methods

3.1. Analysis of structures and landforms

We investigated the structure and landforms of the North Polar Cap with complementary data sets, which have been incorporated into a geographic information system using the Mars 2000 geographic coordinate system and the polar stereographic projection. Topographic information is provided by the Mars Orbiter Laser Altimeter (MOLA). The selected polar digital terrain model has a relative vertical accuracy of 1 m and an average spatial resolution of 512 pixels/° (Smith et al., 2001b). Geomorphological and structural information is provided by (1) images of the Mars Orbiter Camera (MOC) with a spatial resolution of 231 m/pixels (Malin et al., 1992) and (2) images of the Context Camera (CTX) with a spatial resolution of 6 m/pixels over a swath that is about 30 km wide (Malin et al., 2007).

3.2. Analysis of the mineralogical composition

3.2.1. Data

The mineralogical composition of the study area was investigated from data acquired by the OMEGA and CRISM imaging spectrometers. Since we aim at observing sediments in the bulk and at the surface of the permanent ice cap, we use data acquired in summer only (between Ls = 90° and Ls = 115°), in order to minimize the effect of the seasonal CO_2 and H_2O frost coverage (Byrne et al., 2008; Smith et al., 2001a).

OMEGA (Observatoire pour la Minéralogie, l'Eau, les Glaces et l'Activité) (Bibring et al., 2004), onboard Mars Express, acquires hyperspectral images at a spatial resolution ranging from 300 m to 4.8 km/pixels. A spectrum is acquired in 352 spectral channels ranging from 0.38 to 5.2 μm for each pixel of an image, thus producing data cubes. CRISM (Compact Reconnaissance Imaging Spectrometer for Mars, i.e. Murchie et al., 2007) is onboard Mars Reconnaissance Orbiter (MRO). In the targeted hyperspectral mode, CRISM collects

544 spectral channels ranging from 0.36 to 3.9 μm at a spatial resolution ranging from 15 to 19 m/pixels.

We restricted our analysis to the spectral domain comprised between 1.0 and 2.5 μm. In this wavelength range, the solar reflected light dominates the spectrum, and the thermal emission is negligible (Gendrin et al., 2005). This range is also suitable for the detection of hydrated minerals commonly identified on Mars, and is particularly diagnostic for gypsum. In order to avoid the effect of the CRISM smile (Murchie et al., 2007), we studied only the center of the images.

3.2.2. Data reduction

OMEGA and CRISM spectra are acquired remotely through the atmosphere. In order to extract the spectral contribution of the surface only, the atmospheric spectral contribution is removed by using an empirical atmospheric transmission law derived from the ratio between two spectra acquired at the summit and the base of the Olympus Mons volcano, and scaled to the depth of the CO_2 band (Langevin et al., 2005b; McGuire et al., 2009). The CRISM Analysis Toolkit (CAT) also corrects the photometric angles (Murchie et al., 2007). Custom software routines are used for the spatial co-registration of OMEGA and CRISM images.

3.2.3. Mapping the distribution of water ice

Pure water ice exhibits diagnostic absorption bands at 1.04 μm and 1.25 μm, two broad absorption bands between 1.50 μm and 1.66 μm and between 1.96 and 2.05 μm and one band at 2.55 μm. We mapped the distribution of water ice with the calculation of the 1.50 μm absorption band depth. This criterion is defined as follows (Massé et al., 2010):

$$BD(1.50) = 1 - \frac{R(1.50)}{0.7 * R(1.37) + 0.3 * R(1.82)}$$

where R(x) is the value of reflectance corresponding to the wavelength at x μm.

3.2.4. Mapping the distribution of gypsum

Pure gypsum exhibits one absorption band centered at 1.20 μm (due to H_2O combinations), a triplet of absorption bands of progressively decreasing intensity at 1.44, 1.49 and 1.53 μm (due to O–H stretches), a band at 1.74 μm (due to an OH combination), a double band near 1.94 and 1.97 μm (due to H_2O combinations), a broad band centered at 2.2 μm constituted of two narrower components centered at 2.21 and 2.27 μm (due to H_2O combinations and/or S–O stretching overtones), and a band centered at 2.48 μm (due to S–O stretching combinations) (Cloutis et al., 2006, 2008; Massé et al., 2010).

When gypsum is mixed with water ice, diagnostic gypsum absorption bands remain at 1.44, 1.74, 1.94, 2.21, 2.27 and 2.48 μm, but all of these bands are very shallow and may be overlapped by those of water ice (see Fig. 6f in Massé et al., 2010). When the amount of gypsum in the mixture is small, its diagnostic absorption bands turn into faint inflexions in the spectrum. Hence, to detect gypsum in and around the North Polar Cap, we used a spectral derivative method, which has been developed originally to resolve overlapping absorption bands or weak spectral signatures on terrestrial hyperspectral data (Tsai and Philipot, 1998; Verpoorter, 2010). The application to Martian data is described in Massé (2010). The method is based on the assumption that absorption bands appear as local minima or inflexions in spectra. To ensure the identification of all absorption bands, the algorithm thus first detects the wavelengths of all local minima, maxima and inflexions in the spectra of all pixels of a hyperspectral cube. Then it produces, for each identified wavelength, a map of the distribution of pixels where this wavelength corresponds to a local minimum, maximum or inflexion (Verpoorter, 2010). This

method is sensitive to noise and data have been preliminary denoised using the algorithms described in Massé et al. (2010).

4. Results

4.1. Circumpolar Dune Field

4.1.1. Morphological description

The Circumpolar Dune Field is the largest dune field on Mars. It covers a surface area of ~844.000 km^2 and entirely rings the North Polar Cap between 70°N and 85°N (Fig. 1a), constituting a sediment volume of approximately 1300 to 3600 km^3 (Hayward et al., 2010). The densest parts of the Circumpolar Dune Field are mostly composed of transverse dunes and include the regions of Olympia Planum, Hyperboreae Undae, Siton Undae and Abalos Undae (Fig. 1a) (Tanaka and Hayward, 2008; Tsoar et al., 1979). The density of the dune field decreases toward the Gemini Scopuli region (Fig. 1a), where dunes are scattered and are dominantly barchans (Tanaka and Hayward, 2008).

4.1.2. Detection of gypsum

To map gypsum over the whole Circumpolar Dune Field, we compiled a regional mosaic of OMEGA data by using the same cubes as Horgan et al. (2009). This mosaic combines 48 cubes with an initial resolution ranging from 1.5 to 5.4 km/pixels. The final mosaic was produced at a resolution of 1.5 km/pixels.

Fig. 2 displays the regional maps obtained for selected diagnostic gypsum absorption bands. In Fig. 2a, the colored pixels are those where the spectrum displays local minima simultaneously at both 1.94 μm and 2.21 μm. The absorption band at 1.94 μm is typical of hydrated minerals and the absorption band at 2.21 μm is one of the gypsum diagnostic absorption bands (Massé et al., 2010). In Fig. 2b, the colored pixels are those where the spectrum displays local minima simultaneously at both 2.21 μm and 2.27 μm. These two absorption bands constitute the two narrower components of the diagnostic gypsum absorption band centered at 2.2 μm (Massé et al., 2010). Plotting on a single map only those pixels where two diagnostic gypsum absorption bands are detected simultaneously increases the confidence

level in the interpretation that each band is attributable to the presence of gypsum in these pixels.

These regional maps reveal that gypsum is not restricted to Olympia Planum but covers the whole Circumpolar Dune Field (Figs. 1a and 2). Interestingly, the density of pixels where gypsum absorption bands are detected is higher on Olympia Planum. This observation is consistent with the fact that previous detections of gypsum with classical methods based on the computation of spectral criteria were restricted to this area (Langevin et al., 2005a; contoured in red in Fig. 2). The lowest density of pixels where gypsum is detected corresponds to the Gemini Scopuli region, where the density of dunes is also the lowest (Tanaka and Hayward, 2008).

The regional maps also show the occurrence of gypsum on some pixels scattered over the North Polar Cap, in particular near marginal scarps and in some spiral troughs. As we will now discuss using higher resolution data, these occurrences of gypsum on the polar cap are correlated to interior dune fields associated with marginal scarps, and to sedimentary veneers covering spiral troughs.

4.2. Interior dune fields

4.2.1. Morphological description

In addition to the Circumpolar Dune Field, small isolated dune fields are scattered at the surface of the North Polar Cap. These interior dune fields are abundant in the region of Boreales Scopuli but are absent in the region of Gemini Scopuli. Some of these dune fields are connected to the Circumpolar Dune Field, whereas others are enclosed in depressions of the North Polar Cap (Figs. 1a and 3a). All of these interior dune fields lie systematically downslope from marginal scarps that cut through the North Polar Cap (Figs. 1a, 3a and 5a) (Byrne and Murray, 2002; Edgett et al., 2003; Howard, 2000; Massé et al., 2010; Thomas and Weitz, 1989; Warner and Farmer, 2008).

4.2.2. Detection of gypsum

The largest interior dune field is located on the floor of Chasma Boreale (Fig. 1a). The regional map (Fig. 2) shows that gypsum is present in this dune field. However, the resolution of this map is too low to resolve smaller interior dune fields. We therefore applied the
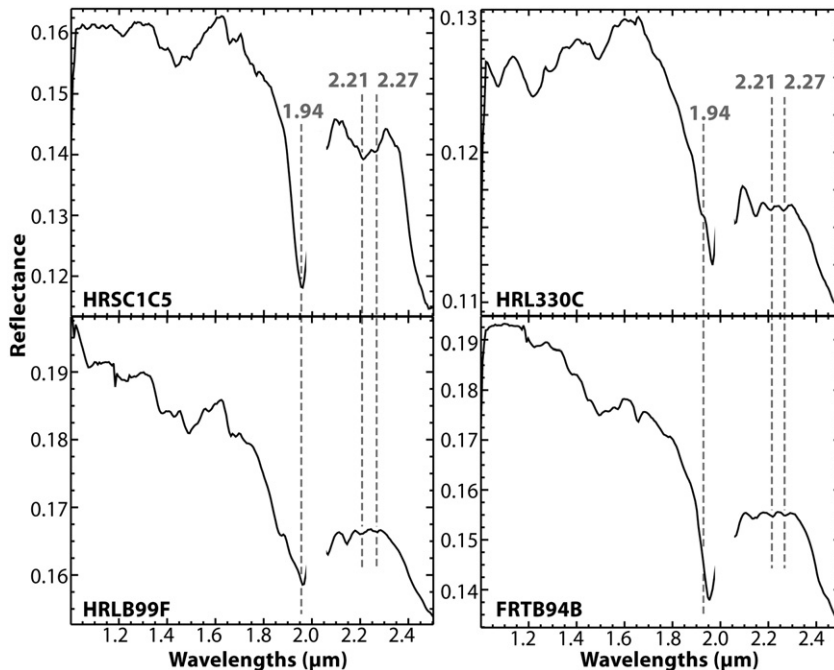

Fig. 4. CRISM spectra acquired on various interior dune fields (location indicated by black crosses in Fig. 3a, CRISM cube label indicated below each spectrum). Gray stippled lines indicate gypsum diagnostic absorption bands (Massé et al., 2010).
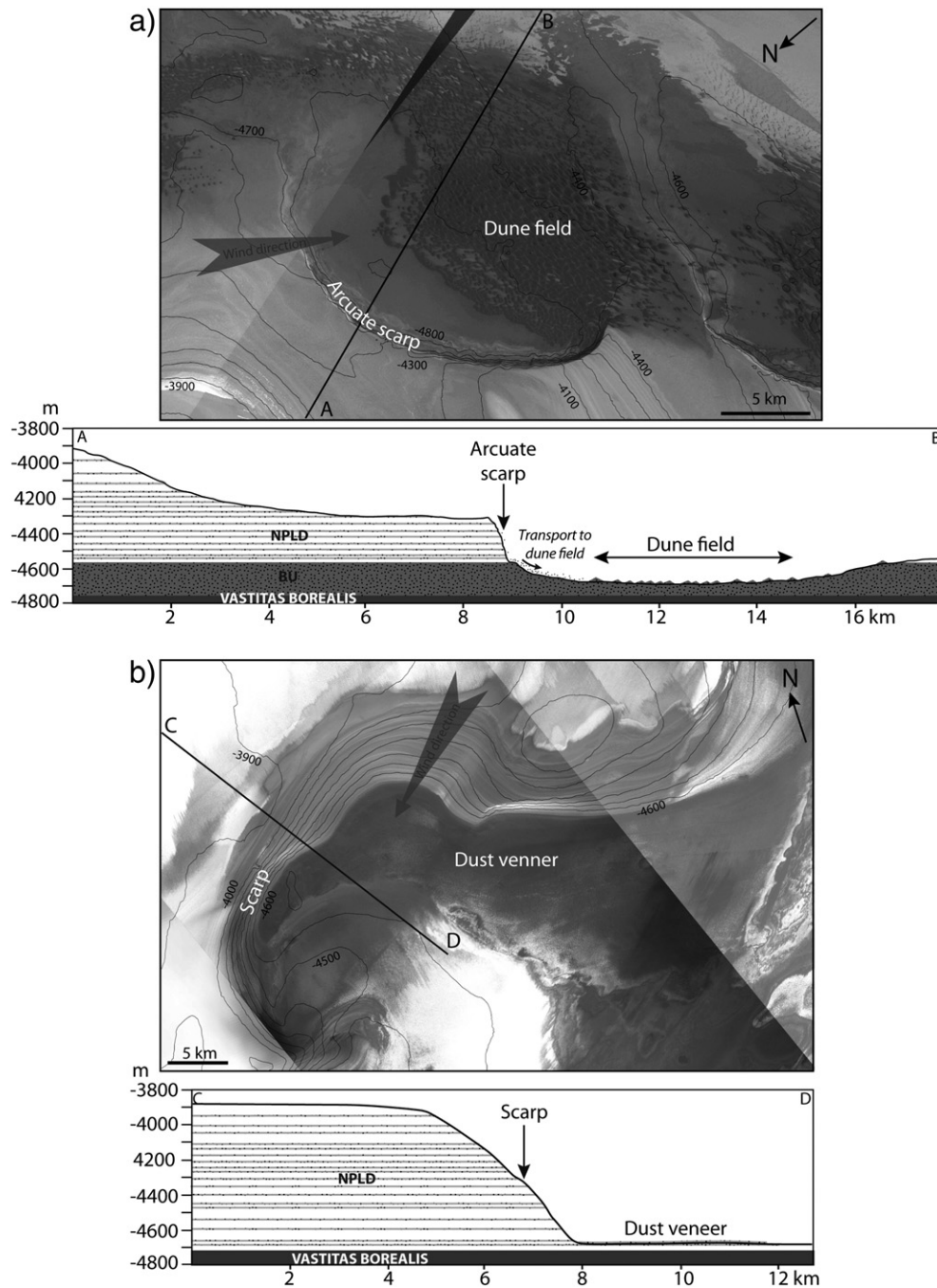
Fig. 5. Maps and interpretative cross-sections of two typical marginal scarps. a) CTX image (# P01_001593_2635) of a scarp located at 119°E in longitude, inside the spatial extent of the BU. b) CTX image (# P01_001531_2600) of a scarp located at 24°E in longitude, outside the spatial extent of the BU. Topographic contours drawn at 100 m intervals from the MOLA DEM at 512 pixels/°. Wind directions inferred from morphological markers indicated by gray arrows.

spectral derivative method to a single OMEGA cube at full spatial resolution (cube number 1030_2, Ls = 111.4°, location indicated in Figs. 1 and 2) that includes most interior dune fields (Fig. 3a, b, c). The simultaneous detection of absorption bands at both 1.94 and 2.21 μm reveals the presence of gypsum in all the interior dune fields (Fig. 3a and b). Absorption bands at both 2.21 and 2.27 μm are also detected simultaneously on these dune fields, but with a more scattered distribution (Fig. 3b and c). This poorer detection is consistent with the fact that the gypsum absorption band at 2.27 μm is shallower than its absorption band at 2.21 μm, particularly when gypsum is mixed with water ice (Massé et al., 2010).

To cross-check the gypsum maps obtained from OMEGA data, we analyzed high-resolution CRISM spectra of selected dune fields

(Figs. 3a and 4). Gypsum absorption bands appear readily on these spectra, which are consistent with laboratory spectra of ice–gypsum mixtures (Massé et al., 2010). These CRISM spectra thus corroborate the detection of gypsum in interior dune fields. They display shallower gypsum absorption bands than spectra acquired on Olympia Planum (e.g., cube hrsc1c5 in Fig. 4) where the gypsum signature was previously identified as being the strongest (Langevin et al., 2005a).

4.3. Sedimentary veneers covering spiral troughs

4.3.1. Morphological description

Spiral troughs in the NPLD have a maximum depth of 800 m and a maximum width of 20 km (Figs. 1a, b and 6). The average slope

gradient of their walls is about 7° and can reach 20° in their steepest parts. NPLD layers are exposed on their steeper-dipping equator-facing slopes, whereas their shallower-dipping pole-facing slopes do not show such layers (Fig. 6g) (Howard et al., 1982). On the basis of these observations, it has been demonstrated that spiral troughs develop by ice ablation on their equator-facing slopes and ice deposition on their pole-facing slopes (Howard, 1978; Howard, 2000; Howard et al., 1982; Ivanov and Muhleman, 2000; Ng and Zuber, 2006). The dominant agent in this process is thought to be katabic winds descending from the polar high toward the ice cap margin (Figs. 6g and 7). These winds would remove ice from the upwind (equator-facing) slopes of the troughs and would carry this material to their downwind (pole-facing) slopes (Fig. 6g). This interpretation has been confirmed recently from SHARAD radar soundings through the NPLD (Smith and Holt, 2010). Equator-facing walls of spiral troughs thus provide natural

cross-sections where ice layers of NPLD, containing various amounts of trapped dust, have been exhumed. Dust trapped in the ice layers has been released by ice ablation along these equator-facing walls, has been transported downwind and has accumulated in the form of thin dust veneers on the floor of spiral troughs and on their pole-facing walls (Howard, 2000; Smith and Holt, 2010).

4.3.2. Detection of gypsum

To determine whether gypsum is present or not in dust released from equator-facing walls of spiral troughs, we analyzed CRISM cube hrs2f12 (Ls = 132.63°, location indicated in Fig. 1a), which encompasses a spiral trough. Fig. 6a displays the water ice map computed from the 1.50 μm band depth. This map shows the presence of nearly pure water ice (in red) on both plateaus flanking the spiral trough. Along the northern (equator-facing) wall of the trough, a
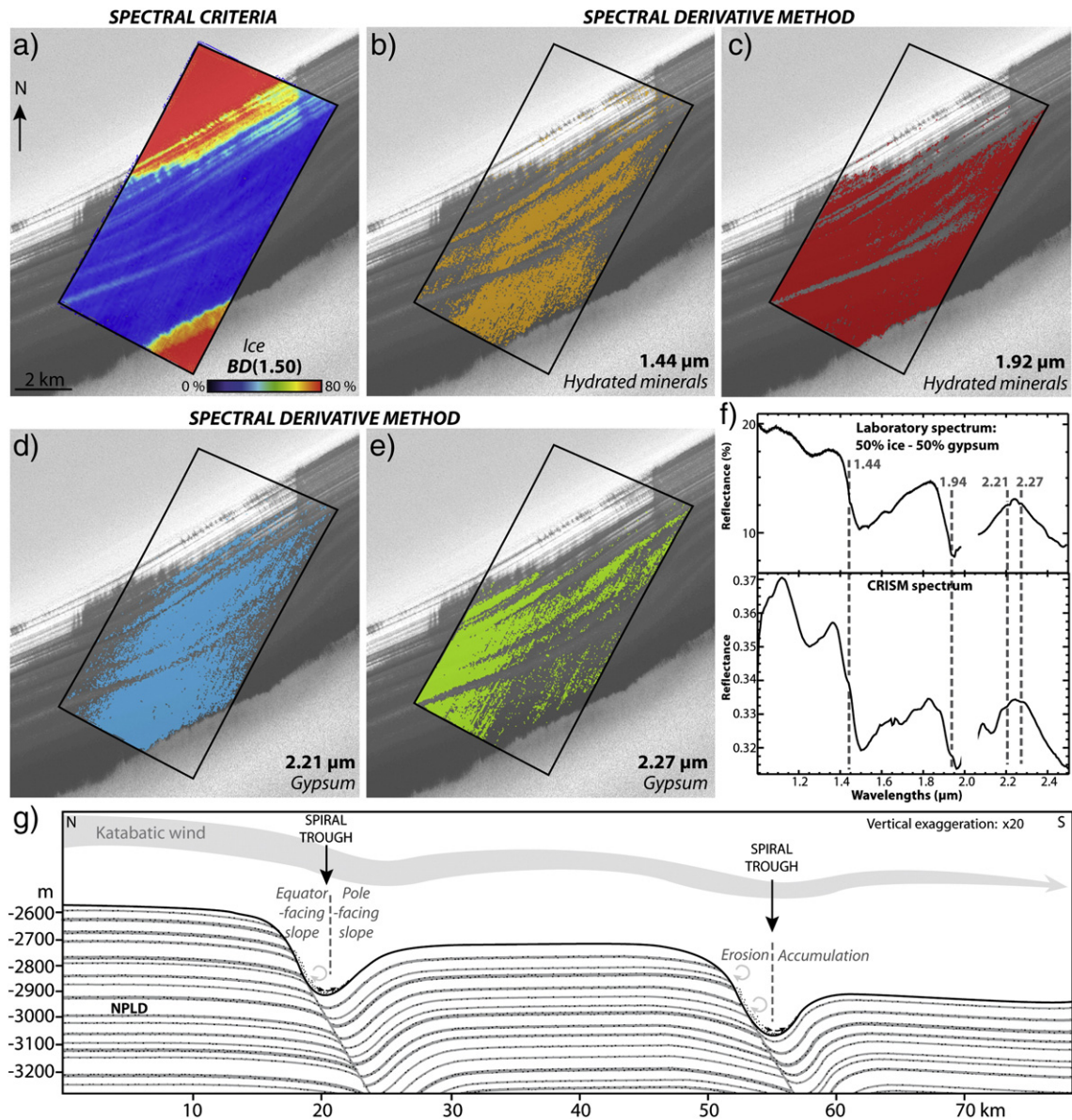
Fig. 6. Distribution of spectral signatures of ice, gypsum and other hydrated minerals on a spiral trough, computed from CRISM cube hrs00002f12. a) Map of spectral criterion BD(1.50). b) to e) Maps of selected inflexions detected by the spectral derivative method. Pixels where the spectrum displays a local inflexion at the considered wavelength are colored. f) Upper part: laboratory spectrum of a mixture of 50% gypsum and 50% water ice (Massé et al., 2010); lower part: CRISM spectrum acquired on a dust-rich ice layer of the pole-facing wall. Both spectra are very similar. The only striking difference is the absorption band at 2.14 μm in the CRISM spectrum; this band has been tentatively attributed to the presence of perchlorate or hannebachite in addition to gypsum in the mixture by Massé et al. (2010). g) Interpretative cross-section of spiral troughs, illustrating how katabatic winds control ice ablation and release of gypsum-bearing sediments from the NPLD along equator-facing walls, and surface accumulation of gypsum-bearing sediments on the floor of spiral troughs and along their pole-facing walls.
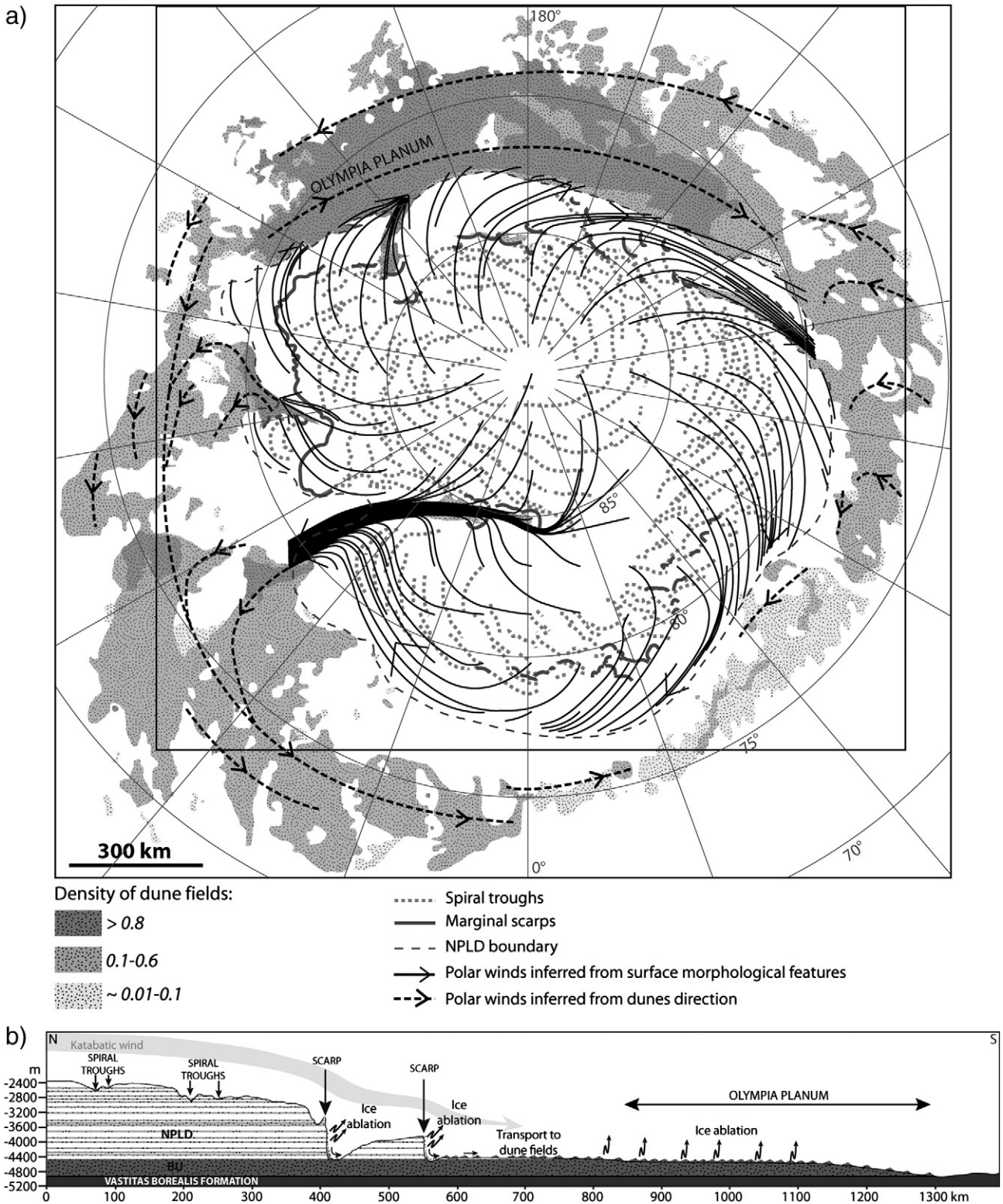
a)

b)

Fig. 7. a) Map of north polar dune fields, spiral troughs and marginal scarps with superimposition of polar wind streamlines interpolated from morphological features observed on the surface of the polar cap (Howard, 2000) and from dunes (Tanaka and Hayward, 2008). b) Interpretative cross-section along an idealized wind streamline, illustrating how katabatic winds and ice ablation control release of gypsum bearing sediments from the BU and the NPLD and accumulation of these sediments in the Circumpolar Dune Field.

package of alternating dust-rich and dust-poor ice layers has been exhumed. Along the southern (pole-facing) wall of the trough, ice layers are not visible because a dust veneer uniformly covers them.

Due to the high amount of water ice mixed with dust in this region, diagnostic gypsum absorption bands appear only as inflexions in CRISM spectra of dust-rich ice layers (Fig. 6f). These inflexions

are consistent with those observed in laboratory spectra of gypsum–ice mixtures containing high ice concentrations (Fig. 6f; Massé et al., 2010). We thus mapped the distribution of gypsum in this area by computing maps of spectral inflexions rather than maps of spectral local minima. We computed these maps for gypsum diagnostic absorption bands at 1.44 μm (Fig. 6b), 1.94 μm (Fig. 6c), 2.21 μm

(Fig. 6d) and 2.27 μm (Fig. 6e). On the resulting maps, the distribution of pixels that display gypsum diagnostic absorption bands is spatially anti-correlated to areas composed of pure water ice (Fig. 6a). Gypsum is observed in dust-rich ice layers exhumed along the equator-facing wall and over the whole dust veneer covering the floor of the spiral trough and its pole-facing wall. It is also observed in dark dust streaks originating in dust-rich-layers and descending the equator-facing wall down to the floor of the trough.

This spectroscopic study of dust released by ablation of ice in a spiral trough thus reveals that dust trapped in the NPLD contains gypsum. This conclusion is consistent with previous spectroscopic detections of gypsum on localized sublimation tills at the surface of the NPLD (Massé et al., 2010).

5. Polar winds

5.1. Reconstruction of winds based on morphological markers

Previous studies have shown that polar winds have a significant impact on the development of spiral troughs, marginal scarps and dune fields over and around the polar cap (Byrne and Murray, 2002; Edgett et al., 2003; Howard, 1978; Howard, 2000; Howard et al., 1982; Ivanov and Muhleman, 2000; Massé et al., 2010; Ng and Zuber, 2006; Smith and Holt, 2010; Tanaka and Hayward, 2008; Thomas and Weitz, 1989; Tsoar et al., 1979; Warner and Farmer, 2008). To emphasize the role of these winds in the release of gypsum bearing sediments from the ice cap and their redistribution in polar dune fields, we compiled a map of polar wind streamlines (Fig. 7a). These streamlines were drawn by interpolating local apparent wind directions derived from directions of frost streaks observed at the surface of the ice cap (Howard, 2000) and those derived from dune morphologies in the Circumpolar Dune Field (Tanaka and Hayward, 2008).

5.2. Interpretation

On the polar cap, wind streamlines (plain black lines in Fig. 7a) turn westward as they descend from the polar high to the margin of the ice cap. This pattern is similar to that observed on Earth in Antarctica (Guo et al., 2002; Parish and Bromwich, 1998). It can be attributed to katabatic winds being deflected westward by the Coriolis force as they descend and accelerate along the slope of the ice cap (Howard, 2000). This is confirmed by mesoscale modeling, i.e. numerical computations of atmospheric winds at fine spatial resolution over a limited area of peculiar interest on the planet (Spiga and Forget, 2009). This simulation has been done in summer because katabatic winds in winter affect probably only the seasonal superficial frost. Moreover, mesoscale modeling reveals that polar winds are nearly unchanging during summer. Simulations in the northern polar cap and surrounding terrains sharing similar settings as in Spiga et al. (2011), Section 7.2, have been thus carried out at Ls = 100° for the purpose of the present study. Fig. 8 shows that the predicted near-surface wind field by mesoscale modeling is in close agreement with wind field inferred from morphological markers in Fig. 7a. It results from an equilibrium between Coriolis force, friction and katabatic acceleration down the slopes of the polar cap. Simulations also show that, contrary to lower-latitude Martian terrains, in polar regions the near-surface katabatic wind structure persists throughout the whole day even in summer. This is most probably due to high thermal inertia over the cap which yields the stable near-surface temperature inversions conducive to katabatic acceleration. In addition, mesoscale modeling indicates that friction velocities of nearly 1 m/s are associated to polar katabatic winds, which suggests plausible erosion and transport of material through those winds.

In the inner part of the Circumpolar Dune Field, close to the ice cap margin, wind streamlines (stippled black lines in Fig. 7a) generally
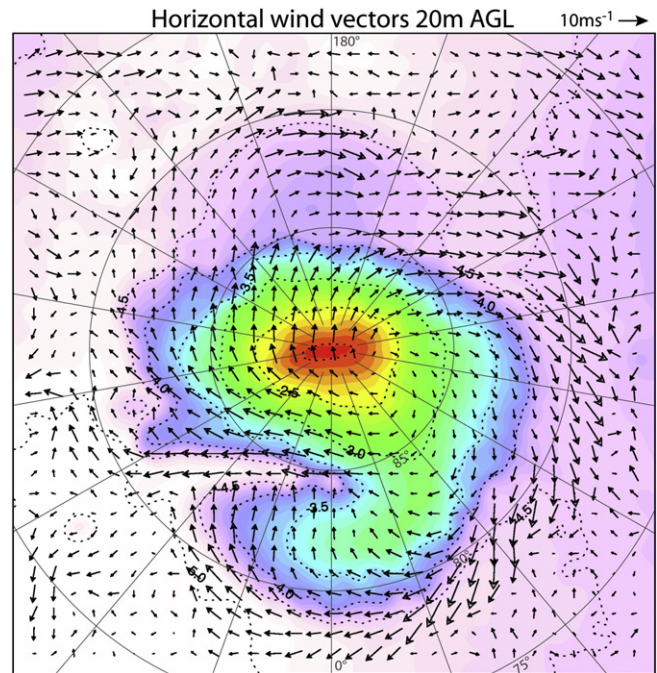

Fig. 8. Summer katabatic winds in the Martian northern polar regions (location indicated by a gray box in Fig. 7a). The figure shows horizontal wind vectors 20 m above local surface (m/s) predicted through mesoscale modeling with 10 km horizontal resolution and polar stereographic projection. Two thirds of the entire simulation domain are shown in the figure. Season is northern summer (Ls = 102°), universal time 09:00 AM. Topography is indicated through color contours. Vectors each 5 grid points.

follow the overall direction of polar katabatic winds and surround the polar cap in a westward turning loop. Further away from the ice cap, in the outer part of the Circumpolar Dune Field, wind streamlines are reversed and form an eastward turning loop. This eastward motion is consistent with zonal wind, which is characterized by a strong eastward blowing jet in the highs latitudes of Mars (Haberle et al., 1993). Local perturbations in these regional wind directions are observed in the Circumpolar Dune Field and can be attributed to seasonal dust storms (Cantor et al., 2010).

6. Discussion

6.1. Wind-driven release of gypsum from the North Polar Cap

The map in Fig. 7a shows the circumpolar and the interior dune fields, the marginal scarps and the spiral troughs. This map reveals that all spiral troughs are perpendicular to wind streamlines. This result is consistent with the hypothesis that katabatic winds control the formation of spiral troughs (Howard, 2000), the release of gypsum bearing sediments from their equator-facing walls and the accumulation of these sediments in the form of superficial veneers covering their pole-facing walls.

Most marginal scarps also are perpendicular to wind streamlines; interior dune fields lie systematically downwind from marginal scarps (Fig. 7a). The link between interior dune fields and marginal scarps thus provides convincing evidence that the source of the dune material is sediment that was initially trapped within the North Polar Cap (Byrne and Murray, 2002; Edgett et al., 2003; Howard, 2000; Thomas and Weitz, 1989; Warner and Farmer, 2008). This gypsum-bearing material has been released from the scarps as the ice retreated by sublimation (Massé et al., 2010). Katabatic winds thus control ice sublimation and gypsum release at marginal scarps and transportation of gypsum-bearing sediments toward interior dune fields.

6.2. Respective contributions of BU and NPLD to gypsum release

It has been unclear so far whether the gypsum-bearing material present in the interior and circumpolar dune fields derives from the whole North Polar Cap, including the NPLD (Herkenhoff and Vasada, 1999; Massé et al., 2010; Thomas and Weitz, 1989), or only from the sediment-rich BU (Fishbaugh and Head, 2005; Herkenhoff et al., 2007). To address this question, we mapped all the scarps that cut through the North Polar Cap (Fig. 1a). These scarps are present all around the North Polar Cap and all face the equator (Howard et al., 1982). From our compilation, we measured that they range from 100 to 1400 m in height (with an average of 720 m), from 8 to 80 km in length (with an average of 30 km) and the slope gradient at their steepest point ranges from 5 to 65° (with an average of 35°).

All scarps that are associated to dune fields display an arcuate shape in map-view (Figs. 1a, 3a and 5a) and have thus been named "arcuate scarps" (Howard, 2000). This arcuate shape has been attributed to preferential undermining of scarp bases because of the presence of sand in the BU (Edgett et al., 2003; Howard, 2000). This interpretation is consistent with the fact that all scarps located in the region of Boreales Scopuli (i.e., within the geographical extent of the BU), display this typical arcuate shape. By contrast, scarps located in the region of Gemini Scopuli (i.e., outside the geographical extent of the BU) have linear or sinuous shapes (Fig. 1a). Interior dune fields are present only in the Boreales Scopuli region, where the BU has been exposed by the development of arcuate scarps (Fig. 1a). A detailed observation thus reveals that interior dune fields are present where scarps have developed sufficiently deep through the NPLD, that they have reached the BU. These particular scarps have a minimal height of 500 m and a minimal slope gradient of 30° at their steepest point.

Some scarps cutting through the NPLD in the Gemini Scopuli region (i.e., outside the geographical extent of the BU) are higher and steeper than the above values, but they are not associated with interior dune fields. For comparison, Fig. 5a and b displays two marginal scarps, located respectively within and outside the geographical extent of the BU, and displaying respective lengths of 26 and 47 km and respective heights of 630 and 785 m. The first one has carved the NPLD down to the BU. It is associated with a gypsum-bearing dune field fed by material released from the scarp (Massé et al., 2010). The second one has carved a similar amount of NPLD, but only a thin veneer of gypsum-bearing sediments is visible at its foot. The closest dunes, which belong to the Circumpolar Dune Field, are more than 150 km apart from the scarp and have no visible connection with it (Fig. 1a).

This observation suggests that erosion of the NPLD merely leads to the formation of thin gypsum-bearing dust veneers, whereas erosion of the BU leads to the formation of gypsum-bearing dune fields. This interpretation is consistent with the presence of a higher concentration of sediment in the BU and a lower concentration of dust particles in the NPLD (Phillips et al., 2008; Picardi et al., 2005; Putzig et al., 2009).

Dunes are composed of sand-sized grains with a diameter of a few hundred microns (Bagnold, 1954). This means either that the gypsum crystals released from the BU are as coarse as a few hundred microns in diameter, or that the grains in the dunes are composed of smaller gypsum crystals aggregated with ice and/or other minerals (Herkenhoff and Vasada, 1999).

6.3. Wind-driven exportation of gypsum toward the Circumpolar Dune Field

The three densest portions of the Circumpolar Dune Field, namely Olympia Undae, Abalos Undae and Hyperboreae Undae, lie downwind from the deepest and longest marginal scarps, namely Olympia Cavi, Rupes Tenuis and Chasma Boreale. These three scarps reach the BU. Other dense areas of the Circumpolar Dune Field lie downwind from (and are connected to) interior dune fields associated with smaller marginal scarps that also reach the BU also (Figs. 1 and 5a). These relations provide evidence that gypsum crystals present in the Circumpolar Dune Field have been released from the BU at marginal scarps and have been exported to their current location by winds. These winds, rotating around the North Polar Cap, are responsible for the redistribution of the gypsum-bearing material all around the margins of the ice cap in the form of the Circumpolar Dune Field (Fig. 5a).

Olympia Cavi is apparently too small however, when compared to Rupes Tenuis and Chasma Boreale, to be responsible for the release of an amount of material sufficient to cover an area as wide as Olympia Planum. Selvans et al. (2010) have recently demonstrated from MARSIS radar data that the BU underlies Olympia Planum (Fig. 1a). It has also been demonstrated that Olympia Planum corresponds to an ancient part of the North Polar Cap, which has been exhumed by erosional retreat of its upper part (Fishbaugh and Head, 2000; Fishbaugh and Head, 2005; Zuber et al., 1998). It can thus be postulated that dunes covering Olympia Planum are dominantly composed of gypsum-bearing material that has been provided in-situ by vertical ablation of the BU (Fig. 7b).

6.4. Spatial variations in intensity of gypsum spectral signatures

Intensities of gypsum spectral signatures are very variable amongst the mapped gypsum-bearing sediments: the strongest signatures occur in Olympia Planum and the faintest ones occur on floors of spiral trough in the NPLD (Figs. 2 and 7). At least three non-exclusive reasons can explain this diversity.

First, regions with the highest density of pixels containing gypsum (Fig. 2) correspond to the densest portions of the Circumpolar Dune Field (Olympia Undae, Abalos Undae and Hyperboreae Undae, Fig. 1a). In regions of the Circumpolar Dune Field where dunes are more scattered (e.g., south of Gemini Scopuli), shallower gypsum detections can be explained by spatial exposures of gypsum being too small to be spatially resolved by the spectro-imager.

Second, the intensity of gypsum absorption bands depends on the amount of gypsum in spectral mixtures (Massé et al., 2010). Thus, areas with the strongest gypsum signatures may correspond to areas containing the greatest amount of gypsum relative to other minerals or to ice.

Third, gypsum absorption bands generally decrease in depth with decreasing grain size (Ghrefat et al., 2007). Now, because gypsum is a very soft mineral (its hardness is 2 on the Mohs scale), gypsum sand grains quickly break down into smaller grains during wind transport (Fishbaugh et al., 2007). For example, in the largest gypsum dune field on Earth (White Sands, New Mexico), gypsum grains decrease in size with increasing distance from their source (Langford, 2003). In the case of the Martian Circumpolar Dune Field, most gypsum grains contained in the dunes of Olympia Planum have been released in-situ from the BU and have probably been transported on short distances only. Therefore they are probably relatively coarse and produce deep absorption bands. On the other hand, the material contained in dunes of the Gemini Scopuli region has probably been transported on long distances, from regions where the BU is present to its present location (Fig. 7). Gypsum grains contained in these dunes are therefore probably smaller due to mechanical erosion and produce shallower absorption bands than those of Olympia Planum.

Similarly, the faintness of gypsum absorption bands on dust veneers that cover the surface of the NPLD in spiral troughs and downwind from marginal scarps that do not cut through the BU can be attributed to smaller grain sizes and to the fact that gypsum is still mixed with large amounts of ice.

7. Conclusion

Previous studies have shown the presence of gypsum on Olympia Planum dunes and of hydrated and mafic minerals on all kinds of

polar superficial sediments (Calvin et al., 2009; Horgan and Bell, 2009; Horgan et al., 2009; Poulet et al., 2008). By the use of a spectral derivative method we find that the hydrated minerals previously detected in all these deposits correspond to gypsum, a hydrated calcium sulfate.

Gypsum is present in thin ablation tills covering the NPLD, especially on floors of spiral troughs. These ablation tills are composed of dust that was previously contained in the NPLD ice layers. Under the influence of katabatic winds, this gypsum-bearing dust has been released by ice ablation on equator-facing slopes of spiral troughs and has accumulated in the form of superficial sedimentary veneers on their pole-facing slopes and more generally over the surface of the North Polar Cap.

Gypsum is also present in thin ablation tills located downwind from marginal scarps that cut through the NPLD but not through the BU. These ablation tills are composed of dust that was released from the NPLD ice layers by wind-driven ice ablation at marginal scarps and has accumulated downwind in the form of thin dust veneers.

Finally, gypsum is present in interior dune fields covering the North Polar Cap and in the whole Circumpolar Dune Field. These gypsum-bearing dune fields lie systematically downwind from marginal scarps that cut down to the BU. From this relation, we infer that the dunes are composed of sand-sized particles containing gypsum that were released from the BU, by horizontal ice ablation at marginal scarps and by vertical ice ablation on Olympia Planum. These particles may be either coarse gypsum crystals, or grains composed of smaller gypsum crystals aggregated with ice and/or other minerals. Katabatic winds descending from the polar high control the release of these particles from the BU and their transportation toward the Circumpolar Dune Field (Fig. 7). Over the Circumpolar Dune Field, the intensity of gypsum diagnostic absorption bands decreases as the downwind distance to the BU increases; this provides evidence either that the gypsum-bearing particles decrease in size during their transportation from the BU toward the Circumpolar Dune Field, or that the amount of gypsum decreases as the downwind distance from the BU increases. Whatever its cause, this downwind decrease in the intensity of gypsum diagnostic absorption bands is consistent with the fact that the BU is the major source of gypsum for the dunes.

This regional study, performed over the whole extent of the North Polar Cap and of the Circumpolar Dune Field, thus confirms that, at the present time on Mars, gypsum crystals are released by ablation of ice deposits forming the NPLD and the BU. More specifically, gypsum observed in the interior and circumpolar dune fields derives mostly from the lower part of the North Polar Cap, namely the BU. This is consistent with the hypothesis that gypsum observed in Olympia Planum derives from the BU (Calvin et al., 2009; Roach et al., 2007). Our work also supports the hypothesis that glacial processes may be responsible for the formation of other sulfate accumulations at lower latitudes on Mars in the past (Massé, 2010; Niles and Michalski, 2009).

Acknowledgments

References

Bagnold, R.A., 1954. The Physic of Blown Sand and Desert Dunes. Dover Publications. 265pp.

Bibring, J.-P., Soufflot, A., Berthé, M., Langevin, Y., Gondet, B., Drossart, P., Bouyé, M., Combes, M., Puget, P., Semery, A., Bellucci, G., Formisano, V., Moroz, V., Kottsov, V., Bonello, G., Erard, S., Forni, O., Gendrin, A., Manaud, N., Poulet, F., Poulleau, G., Encrenaz, T., Fouchet, T., Melchiori, R., Altieri, F., Ignatiev, N., Titov, D., Zasova, L., Coradini, A., Capacionni, F., Cerroni, P., Fonti, S., Mangold, N., Pinet, P., Schmitt, B., Sotin, C., Hauber, E., Hoffman, H., Jaumann, R., Keller, U., Arvidson, R., Mustard, J., Forget, F., 2004. OMEGA: Observatoire pour la Minéralogie, l'Eau, les Glaces et l'Activité. Eur. Space Agency Spec. Publ. 1240, 37.

Byrne, S., Murray, B.C., 2002. North polar stratigraphy and the paleo-erg of Mars. J. Geophys. Res. 107 (E6), 5044. doi:10.1029/2001JE001615.

Byrne, S., Zuber, M.T., Neumann, G.A., 2008. Internannual and seasonal behavior of Martian residual ice-cap albedo. Planet. Space Sci. 56, 194–211.

Calvin, W.M., Roach, L.H., Seelos, F.P., Seelos, K.D., Green, R.O., Murchie, S.L., Mustard, J.F., 2009. CRISM observations of the northern Martian latitudes in summer. J. Geophys. Res. 114, E00D11. doi:10.1029/2009JE003348.

Cantor, B.A., James, P.B., Calvin, W.M., 2010. Marci and MOC observations of the atmosphere and surface cap in the north polar region of Mars. Icarus 208, 61–81.

Carr, M.H., Head, J.W., 2009. Geologic history of Mars. Earth Planet. Sci. Lett. doi:10.1016/j.epsl.2009.06.042

Cloutis, E.A., Hawthorne, F.C., Mertzman, S.A., Krenn, K., Craig, M.A., Marcino, D., Methot, M., Strong, J., Mustard, J.F., Blaney, D.L., Bell III, J.F., Vilas, F., 2006. Detection of sulfate minerals using reflectance spectroscopy. Icarus 184, 121–157.

Cloutis, E.A., Craig, M.A., Kruzelecky, R.V., Jamroz, W.R., Scott, A., Hawthorne, F.C., Mertzman, S.A., 2008. Spectral reflectance properties of minerals exposed to simulated Mars surface conditions. Icarus 195, 140–168.

Edgett, K.S., Williams, R.M.E., Malin, M.C., Cantor, B.A., Thomas, P.C., 2003. Mars landscape evolution: influence of stratigraphy in the north polar region. Geomorphology 52, 289–297.

Fishbaugh, K.E., Head III, J.W., 2000. North polar region of Mars: Topography of circumpolar deposits from Mars Orbiter Laser Altimeter (MOLA) data and evidence for asymmetric retreat of the polar cap. J. Geophys. Res. 105, 22455–22486.

Fishbaugh, K.E., Head III, J.W., 2005. Origin and characteristics of the Mars north polar basal unit and implications for polar geologic history. Icarus 174, 444–474.

Fishbaugh, K.E., Poulet, F., Chevrier, V., Langevin, Y., Bibring, J.-P., 2007. On the origin of gypsum in the Mars north polar region. J. Geophys. Res. 112, E07002. doi:10.1029/2006JE002862.

Fishbaugh, K.E., Hvidberg, C.S., Beaty, D., Clifford, S., Fisher, D., Haldemann, A., Head, J.W., Hecht, M., Koutnik, M., Tanaka, K., Ammann, W.J., 2008. Introduction to the 4th Mars Polar Science and Exploration Conference special issue: five top questions in Mars polar science. Icarus 196, 305–317.

Gendrin, A., Mangold, N., Bibring, J.-P., Langevin, Y., Gondet, B., Poulet, F., Bonello, G., Quantin, C., Mustard, J., Arvidson, R., Le Mouélic, S., 2005. Sulfates in Martian layered terrains: the OMEGA/Mars Express view. Science 307, 1587–1591.

Ghrefat, H.A., Goodell, P.C., Hubbard, B.E., Langford, R.P., Aldouri, R.E., 2007. Modeling grain size variations of Aeolian gypsum deposits at White Sands, New Mexico, using AVIRIS imagery. Geomorphology 88, 57–68.

Grima, C., Kofman, W., Mouginot, J., Phillips, R.J., Hérique, A., Biccari, D., Seu, R., Cutigini, M., 2009. North polar deposits of Mars: extreme purity of the water ice. GRL 36, L03203. doi:10.1029/2008GL036326.

Guo, Z., Bromwich, D., Cassano, J.J., 2002. Evaluation of Polar MM5 simulations of Antarctic atmospheric circulation. Mon. Weather Rev. 131, 384–411.

Haberle, R.M., Pollack, J.B., Barnes, J.R., Zurek, R.W., Leovy, C.B., Murphy, J.R., Lee, H., Schaeffer, J., 1993. Mars atmospheric dynamics as simulated by the NASA AMES general circulation model. I — the zonal-mean circulation. J. Geophys. Res. 98, 3093–3123.

Hayward, R.K., Fenton, L.K., Tanaka, K.L., Titu, s T.N., Christensen, P.R., 2010. Mars global digital dune database: dune volume estimates in the North Polar region. 41st LPSC, Abstract 1109.

Herkenhoff, K.E., Vasada, A.R., 1999. Dark material in the polar layered deposits and dunes on Mars. J. Geophys. Res. 104 (16), 487–16,500.

Herkenhoff, K.E., Byrne, S., Russell, P.S., Fishbaugh, K.E., McEwen, A.S., 2007. Meter-scale morphology of the North Polar Region of Mars. Science 317, 1711–1715.

Horgan, B.H., Bell III, J.F., 2009. Insights from ferrous mineralogy into the transport of Martian north polar materials. 40th LPSC, Abstract 2457.

Horgan, B.H., Bell III, J.F., Noe Dobrea, E.Z., Cloutis, E.A., Bailey, D.T., Craig, M.A., Roach, L.H., Mustard, J.F., 2009. Distribution of hydrated minerals on the north polar region of Mars. J. Geophys. Res. 114, E01005. doi:10.1029/2008JE003187.

Howard, A.D., 1978. Origin of the stepped topography of the Martian poles. Icarus 34, 581–599.

Howard, A.D., 2000. The role of eolian processes in forming surface features of the Martian Polar Layered Deposits. Icarus 144, 267–288. doi:10.1006/icar.1999.6305.

Howard, A.D., Cutts, J.A., Blasius, K.R., 1982. Stratigraphic relationships within Martian polar cap deposits. Icarus 50, 161–215.

Iizuka, Y., Hondoh, T., Fujii, Y., 2006. Na$_2$SO$_4$ and MgSO$_4$ salts during the Holocene period derived by high-resolution depth analysis of a Dome Fuji ice core. J. Glaciol. 52 (176).

Iizuka, Y., Horikawa, S., Sakurai, T., Johnson, S., Dahl-Jensen, D., Steffensen, J.P., Hondoh, T., 2008. A relationship between ion balance and the chemical compounds of salt inclusions found in the Greenland Ice Core Project and Dome Fuji ice cores. J. Geophys. Res. 113, D07303. doi:10.1029/2007JD009018.

Ivanov, A.B., Muhleman, D.O., 2000. The roles of sublimation for the formation of the northern ice cap: results from the Mars Orbiter Laser Altimeter. Icarus 144, 436–448.

Kieffer, H.H., Chase, S.C., Martin, T.Z., Miner, E.D., Don Palluconi, F., 1976. Martian North Pole summer temperature: dirty water ice. Science 194, 1341–1344.

Langevin, Y., Poulet, F., Bibring, J.-P., Gondet, B., 2005a. Sulfates in the North Polar Region of Mars detected by OMEGA/Mars Express. Science 307, 1584–1586.

Langevin, Y., Poulet, F., Bibring, J.-P., Schmitt, B., Douté, S., Gondet, B., 2005b. Summer evolution of the North Polar Cap of Mars as observed by OMEGA/Mars Express. Science 307, 1581–1584.

Langford, R.P., 2003. The Holocene history of White Sands dune fields and influences on eolian deflation and playa lakes. Quat. Int. 104, 31–39.

Malin, M.C., Danielson, G.E., Ingersoll, A.P., Veverka, H.J., Ravine, M.A., Soulanille, T.A., 1992. Mars Observer Camera. J. Geophys. Res. 112, E05S02. doi:10.1029/2005JE002605.

Malin, M.C., Bell, J.F., Cantor, B.A., Caplinger, M.A., Calvin, W.M., Clancy, R.T., Edgett, K.S., Edwards, L., Haberle, R.M., James, P.B., Lee, S.W., Ravine, M.A., Thomas, P.C., Wolff, M.J., 2007. Context Camera Investigation on board the Mars Reconnaissance Orbiter. J. Geophys. Res. 112, E05S04. doi:10.1029/2006JE002808.

Massé, M., 2010. Nature et Origine des Dépôts de Sulfates dans les Régions Équatoriales et Polaires de Mars. Comparaison Morphologique et Minéralogique entre Aram Chaos et la Calotte Polaire Nord. Unpublished PhD Thesis, University of Nantes, Nantes (France), 298 p.

Massé, M., Bourgeois, O., Le Mouélic, S., Verpoorter, C., Le Deit, L., Bibring, J.-P., 2010. Martian polar and circum-polar sulfate-bearing deposits: sublimation tills derived from the North Polar Cap. Icarus. doi:10.1016/j.icarus.2010.04.017.

McGuire, P.C., Bishop, J.L., Brown, A.J., Fraeman, A.A., Marzo, G.A., Morgan, M.F., Murchie, S.L., Mustard, J.F., Parente, M., Pelkey, S.M., Roush, T.L., Seelos, F.P., Smith, M.D., Wendt, L., Wolff, M.J., 2009. An improvement to the volcano-scan algorithm for atmospheric correction of CRISM and OMEGA spectral data. Planet. Space Sci. 57, 809–815.

Murchie, S., Arvidson, R., Bedini, P., Beisser, K., Bibring, J.-P., Bishop, J., Boldt, J., Cavender, P., Choo, T., Clancy, R.T., Darlington, E.H., Des Marais, D., Espiritu, R., Fort, D., Green, R., Guiness, E., Hayes, J., Hash, C., Heffernan, K., Hemmler, J., Hayler, G., Humm, D., Hutcheson, J., Izenberg, N., Lee, R., Lees, J., Lohr, D., Malaret, E., Martin, T., McGovern, J.A., McGuire, P., Morris, R., Mustard, J., Palkey, S., Rhodes, E., Robinson, M., Roush, T., Schaeffer, E., Seagrave, G., Seelos, F., Silvergate, P., Slavney, S., Smith, M., Shyong, W.-J., Strohbehn, K., Taylor, H., Thompson, P., Tossman, B., Wirzburger, M., Wolff, M., 2007. Compact Reconnaissance Imaging Spectrometer for Mars (CRISM) on Mars Reconnaissance Orbiter (MRO). J. Geophys. Res. 112 (E5), E05S03. doi:10.1029/2006JE002682.

Ng, F.S.L., Zuber, M.T., 2006. Patterning instability of the Mars polar ice caps. J. Geophys. Res. 111, E02005. doi:10.1029/2005JE002533.

Niles, P., Michalski, J., 2009. Meridiani Planum sediments on Mars formed through weathering in massive ice deposits. Nat. Geosci. 2, 215–220.

Ohno, H., Igarashi, M., Hondoh, T., 2006. Characteristics of salt inclusions in polar ice from Dome Fuji, East Antarctica. Geophys. Res. Lett. 113, L08501. doi:10.1029/2006GL025774.

Parish, T.R., Bromwich, D.H., 1998. A case study of Antarctic katabatic wind interaction with large-scale forcing. Mon. Weather Rev. 126, 199–206.

Phillips, R.J., Zuber, M.T., Smrekar, S.E., Mellon, M.T., Head, J.W., Tanaka, K.L., Putzig, N.E., Milkovich, S.M., Campbell, B.A., Plaut, J.J., Safaeinili, A., Seu, R., Biccari, D., Carter, L.M., Picardi, G., Orosei, R., Mohit, P.S., Heggy, E., Zurek, R.W., Egan, A.F., Giacomoni, E., Russo, F., Cutigni, M., Pettinelli, E., Holt, J.W., Leuschen, C.J., Marinangelli, L., 2008. Mars north polar deposits: stratigraphy, age, and geodynamical response. Science 320, 1182–1185.

Picardi, G., Plaut, J.J., Biccari, D., Bombaci, O., Calabrese, D., Cartacci, M., Ciccetti, A., Clifford, S.M., Edenhoffer, P., Farell, W.M., Federico, C., Frigeri, A., Gurnett, D.A., Hagfors, T., Haggy, E., Herique, A., Huff, R.L., Ivanov, A.B., Johnson, W.T.K., Jordan, R.L., Kirchner, D.L., Kofman, W., Lauschen, C.J., Nielsen, E., Orosei, R., Pettinelli, E., Phillips, R.J., Plettemeier, D., Safaenili, A., Seu, R., Stofan, E.R., Vannaroni, G., Watters, T.R., Zampilini, E., 2005. Radar sounding of the subsurface of Mars. Science 310, 1925–1928.

Poulet, F., Langevin, Y., Boubin, G., Jouglet, D., Bibring, J.-P., Gondet, B., 2008. Spectral variability of the Martian high latitude surfaces. Geophys. Res. Lett. 35, L20201. doi:10.1029/2008GL035450.

Putzig, N.E., Phillips, R.J., Campbell, B.A., Holt, J.W., Plaut, J.J., Carter, L.M., Egan, A.F., Bernardini, F., Saefaeinili, A., Seu, R., 2009. Subsurface structure of Planum Boreum from Mars Reconnaissance Orbiter shallow radar soundings. Icarus. doi:10.1016/j.icarus.2009.07.034.

Roach, L.H., Mustard, J.F., Murchie, S., Langevin, Y., Bibring, J.-P., Bishop, J., Bridges, N., Brown, A., Byrne, S., Ehlmann, B.L., Herkenhoff, K., McGuire, P.C., Milliken, R.E., Pelkey, S., Poulet, F., Seelos, F.P., Seelos, K., CRISM Team, 2007. CRISM spectral signatures of the North polar gypsum dunes. LPSC XXXVII, Abstract.

Selvans, M.M., Plaut, J.J., Aharonson, O., Safaeinili, A., 2010. Internal structure of Planum Boreum, from Mars Advanced Radar for Subsurface and Ionospheric Sounding data. J. Geophys. Res. 115, E09003.

Smith, I.B., Holt, J.W., 2010. Onset and migration of spiral troughs on Mars revealed by orbital radar. Nature 465, 450–453. doi:10.1038/nature09049.

Smith, D.E., Zuber, M.T., Neumann, G.A., 2001a. Seasonal variations of snow depth on Mars. Science 294 (5549), 2141–2146.

Smith, D.E., Zuber, M.T., Frey, H.V., Garvin, J.B., Head, J.W., Muhleman, D.O., Pettengill, G.H., Phillips, R.J., Solomon, S.C., Zally, H.J., Banerdt, W.B., Duxbury, T.C., Golombek, M.P., Lemoine, F.G., Neumann, G.A., Rowlands, D.D., Aharonson, O., Ford, P.G., Ivanov, A.B., Johnson, C.L., McGovern, P.J., Abshire, J.B., Afzal, R.S., Sun, X., 2001b. Mars Orbiter Laser Altimeter (MOLA): experiment summary after the first year of global mapping of Mars. J. Geophys. Res. 106, 23689–23722.

Spiga, A., Forget, F., 2009. A new model to simulate the Martian mesoscale and micro-scale atmospheric circulation: validation and first results. J. Geophys. Res. 114, E02009.

Spiga, A., Forget, F., Madeleine, J.-B., Montabone, L., Lewis, S.R., Millour, E., 2011. The impact of Martian mesoscale winds on surface temperature and the determination of thermal inertia. Icarus 212, 504–519.

Szynkiewicz, A., Ewing, R.C., Moore, C.H., Glamoclija, M., Bustos, D., Pratt, L.M., 2010. Origin of terrestrial gypsum dunes—implications for Martian gypsum-rich dunes of Olympia Undae. Geomorphology 121, 69–83.

Tanaka, K.L., Hayward, R.K., 2008. Mars' North circum-polar dunes: distribution, sources, and migration history. Planetary Dunes Workshop: A Record of Climate Change, Abstract 7012.

Tanaka, K.L., Rodriguez, J.A.P., Skinner, J.A., Bourke, M.C., Fortezzo, C.M., Herkenhoff, K.E., Kolb, E.J., Okubo, C.H., 2008. North polar region of Mars: advances in stratigraphy, structure, and erosional modification. Icarus 196, 318–358.

Thomas, P., Weitz, C., 1989. Sand dune materials and polar layered deposits on Mars. Icarus 81, 185–215.

Tsai, F., Philipot, W., 1998. Derivative analysis of hyperspectral data. Remote. Sens. Environ. 66 (1), 41–51.

Tsoar, H., Greeley, R., Peterfreund, A.R., 1979. Mars: the north polar sand sea and related wind patterns. J. Geophys. Res. 84, 8167–8180.

Verpoorter, C., 2010. Teledetection Hyperspectrale Et Cartographie Des Facies Sedimentaires. In: Editions Universitaires Europeennes (Ed.), . ISBN: 9786131552113, p. 516.

Warner, N.H., Farmer, J.D., 2008. Importance of Aeolian processes in the origin of the north polar chasmata, Mars. Icarus 196, 368–384.

Zuber, M., Smith, D.E., Solomon, S.C., Abshire, J.B., Afzal, R.S., Aharonson, O., Fishbaugh, K., Ford, P.G., Frey, H.V., Garvin, J.B., Head, J.W., Ivanov, A.B., Johnson, C.L., Muhleman, D.O., Neumann, G.A., Pettengill, G.H., Phillips, R.J., Sun, X., Zwally, H.J., Banerdt, W.B., Duxbury, T.C., 1998. Observations of the north polar region of Mars from the Mars Orbiter Laser Altimeter. Science 282, 2053–2060.